Chin. Geogra. Sci. 2022 Vol. 32 No. 1 pp. 127−141
https://doi.org/10.1007/s11769-021-1250-4

Springer Science Press
www.springerlink.com/content/1002-0063

Modeling Spatio-temporal Drought Events Based on Multi-temporal, Multi-source Remote Sensing Data Calibrated by Soil Humidity

LI Hanyu[1], KAUFMANN Hermann[2], XU Guochang[1]

(1. *Institute of Space Science and Applied Technology*, *Harbin Institute of Technology* (*Shenzhen*), *Shenzhen* 518000, *China*; 2. *Remote Sensing Section*, *German Research Centre for Geosciences* (*GFZ*), *Potsdam* 14473, *Germany*)

Abstract: Inspired by recent significant agricultural yield losses in the eastern China and a missing operational monitoring system, we developed a comprehensive drought monitoring model to better understand the impact of individual key factors contributing to this issue. The resulting model, the 'Humidity calibrated Drought Condition Index' (HcDCI) was applied for the years 2001 to 2019 in form of a case study to Weihai County, Shandong Province in East China. Design and development are based on a linear combination of the Vegetation Condition Index (VCI), the Temperature Condition Index (TCI), and the Rainfall Condition Index (RCI) using multi-source satellite data to create a basic Drought Condition Index (DCI). VCI and TCI were derived from MODIS (Moderate Resolution Imaging Spectroradiometer) data, while precipitation is taken from CHIRPS (Climate Hazards Group InfraRed Precipitation with Station data) data. For reasons of accuracy, the decisive coefficients were determined by the relative humidity of soils at depth of 10–20 cm of particular areas collected by an agrometeorological ground station. The correlation between DCI and soil humidity was optimized with the factors of 0.53, 0.33, and 0.14 for VCI, TCI, and RCI, respectively. The model revealed, light agricultural droughts from 2003 to 2013 and in 2018, while more severe droughts occurred in 2001 and 2002, 2014–2017, and 2019. The droughts were most severe in January, March, and December, and our findings coincide with historical records. The average temperature during 2012–2019 is 1°C higher than that during the period 2001–2011 and the average precipitation during 2014–2019 is 192.77 mm less than that during 2008–2013. The spatio-temporal accuracy of the HcDCI model was positively validated by correlation with agricultural crop yield quantities. The model thus, demonstrates its capability to reveal drought periods in detail, its transferability to other regions and its usefulness to take future measures.

Keywords: comprehensive drought model; condition indices; multi-source satellite data; agricultural drought; soil humidity

Citation: LI Hanyu, KAUFMANN Hermann, XU Guochang, 2022. Modeling Spatio-temporal Drought Events Based on Multi-temporal, Multi-source Remote Sensing Data Calibrated by Soil Humidity. *Chinese Geographical Science*, 32(1): 127−141. https://doi.org/10.1007/s11769-021-1250-4

1 Introduction

The increase in the frequency of droughts in the past has become a prominent problem for cultivation areas with serious economic losses all over the world. As weather extremes are expected to increase even further in the future, adapting agriculture to climate change, especially to higher temperatures and less precipitation, is crucial. Droughts, a common hydrometeorological phenomenon (Wardlow et al., 2012), cause various degrees of harm to the social economy. A severe drought will not only significantly reduce the agricultural yield, but also af-

Received date: 2021-04-16; accepted date: 2021-08-01
Foundation item: Under the auspices of Shenzhen Science and Technology Program (No. KQTD20180410161218820), Guangdong Basic and Applied Basic Research Foundation (No. 2021A1515012600)
Corresponding author: LI Hanyu. E-mail: lihanyu608608@163.com

fect people's economic situation and lives. Drought is a phenomenon that is difficult to quantify and analyze. It has no unified definition and no clear start and stop signs. The simplest manifestation is that the precipitation is less than the normal (West et al., 2019). Traditional drought monitoring methods focus on site-based measurements such as the Palmer Drought Severity Index (PDSI) (Palmer, 1965) and others. The calculation of these indices mainly depends on the measured data of precipitation and or temperature variations. But owing to the usual limited number of meteorological stations and the typical uneven spatial distribution, especially in high altitude and sparsely populated areas, the scale and spatial accuracy of drought studies is limited. With the development of remote sensing technologies, drought monitoring methods have undergone a major transformation. Using remotely sensed data acquired by aircraft or satellite platforms can not only obtain diverse meteorological data, but also monitor the status and the properties of the Earth's surface. The emerging technologies and associated methods have changed the scope of drought monitoring, improved latency, and reduced costs, thereby allowing us to make efficient observations on a larger space-time scale (Choi et al., 2013).

Meteorological drought is often an early indicator of drought disasters, while precipitation monitoring is paramount to this issue. The introduction of remote sensing precipitation products has changed the efficiency and spatial and temporal coverage of precipitation monitoring, but the calculation of precipitation indices requires long-term monitoring data such as the Rainfall Anomaly Index (RAI) (Van Rooy, 1965), the Standardized Precipitation Index (SPI) (McKee et al., 1993), or the Precipitation Condition Index (PCI) (Zhang et al., 2013). The temperature of the soil surface or vegetation canopy affects transpiration and evapotranspiration and hence the water content and balance. To detect even subtle changes in the surface temperature, the wavelengths of the thermal infrared are well suited. Commonly used thermal infrared models are: the Crop Water Stress Index (CWSI) (Idso et al., 1981), the Apparent Thermal Inertia (ATI) (Price, 1985), the Temperature Condition Index (TCI) (Kogan, 1995a), and the Normalized Difference Temperature Index (NDTI) (McVicar and Jupp, 2002). Vegetation is another important factor that has a strong influence on the development of droughts. It is very sensitive to soil moisture, so drought monitoring can be conducted indirectly by detecting the occurrence, distribution and the status of vitality of vegetation. Commonly used vegetation indices are the Normalized Difference Vegetation Index (NDVI) (Rouse et al., 1974), the Enhanced Vegetation Index (EVI) (Huete et al., 1997), the Anomaly Vegetation Index (AVI) (Chen et al., 1994), the Vegetation Condition Index (VCI) (Kogan, 1995b), and the Standard Vegetation Index (SVI) (Qi et al., 2004). As far as microwave remote sensing is concerned, the measurable dielectric properties of soils are directly affected by the moisture content. Thus, a statistical function of soil moisture and backscatter coefficient can be established and the soil moisture can be retrieved from the backscatter coefficient.

Owing to the limitation of a single indicator, many researchers are exploring comprehensive models of multiple indicators in order to improve the accuracy of drought monitoring. Diverse studies have shown that different monitoring indicators and sensors have their specific advantages and disadvantages. Comprehensive models need to adjust the parameters according to the research area, while the regional adaptability is weak. Against this background, Kogan (2002) proposed the Vegetation Health Index (VHI), a weighted average of VCI and TCI that significantly improved the results based on the independent NDVI. Sandholt et al. (2002) proposed the Temperature Vegetation Drought Index (TVDI) based on the empirical relationship between the NDVI and Land Surface Temperature (LST). Du et al. (2013) proposed a Synthesized Drought Index (SDI), combining PCI, TCI, and VCI, in tandem with a principal component analysis to comprehensively evaluate the lack of precipitation, soil water depletion, and vegetation stress. Rhee et al. (2010) combined the LST and NDVI products of the Medium Resolution Imaging Spectrometer (MODIS) and the precipitation data of the Tropical Rainfall Measuring Mission (TRMM) to construct a regional Scaled Drought Condition Index (SDCI), that is suitable for arid and humid areas through a linear weighted combination.

In recent years, China has experienced frequent drought disasters throughout the entire country (Li et al., 2015; Lu et al., 2018). Especially Weihai County, a district in the eastern Shandong Province, faced increasing drought periods that have become a severe problem for the agricultural crop yield and the economic perform-

ance in the area (Bureau of Statistics of Weihai, 2002–2020). In order to understand the increasing frequency of drought periods in the Shandong Province and to be able to take appropriate measures for the future, a transferable remote sensing-based monitoring system is being designed and developed. In this context, we deployed MOD11A1, MOD13Q1, and CHIRPS (Climate Hazards Group InfraRed Precipitation with Station data) data to calculate VCI, TCI and the Rainfall Condition Index (RCI) of the study area. Based on these fundamental indices, we developed a comprehensive model, the 'Humidity calibrated Drought Condition Index' (HcDCI), where the 10–20 cm top soil moisture data of an agrometeorological station were used to determine a combination of weight coefficients suitable for the investigated area and the cultivated crops. The main innovations of this approach can be found in the choice of CHIRPS precipitation data and the calibration using highly reliable soil moisture data, which has been realized seldomly for drought model generation before.

2 Materials and Methods

2.1 Study area

Weihai County is a prefecture-level district at the easternmost edge of the Shandong Province, China, located at a peninsula, between 36°41′N to 37°35′N, 121°11′E to 122°42′E (Fig. 1). In the north, east, and the south, it is bounded by the Yellow Sea. Weihai County is an aggregation of four districts of mostly non-urban character. These are: Rushan, Wendeng, Rongcheng, and Huancui. The administrative capital is the town of Weihai located at the north coast of the Huancui District. Weihai County extends 135 km from east to west and 81 km from north to south, and it has a coastline of 986 km. The total area covers about 5800 km^2. Weihai County is a hilly area with relatively gentle terrains, wide valleys, and low slopes with an average altitude of 63.13 m. The highest peak is the top peak of the Kunyu Mountain, the Talang Peak located west of the Wendeng District with an altitude of 922.8 m. Weihai County belongs to the continental climate of the north temperate monsoon type that is usually characterized by abundant preciptation and moderate annual temperatures. Most of the farmland in Weihai County is rainfed and as such prone to drought events caused by uneven distributed precipitation, the more when temperatures are rising. As the entire area is known for its intensive agricultural activities, drought events have a significant impact on the crop yield and the economic development of the region. A regular monitoring of the affected area with a potential for reliable predictions can help to adjust to the situation at an early stage.

2.2 Data sources

This study is based on the use and analysis of multi-source remote sensing satellite data, including MODIS (Moderate Resolution Imaging Spectroradiometer),

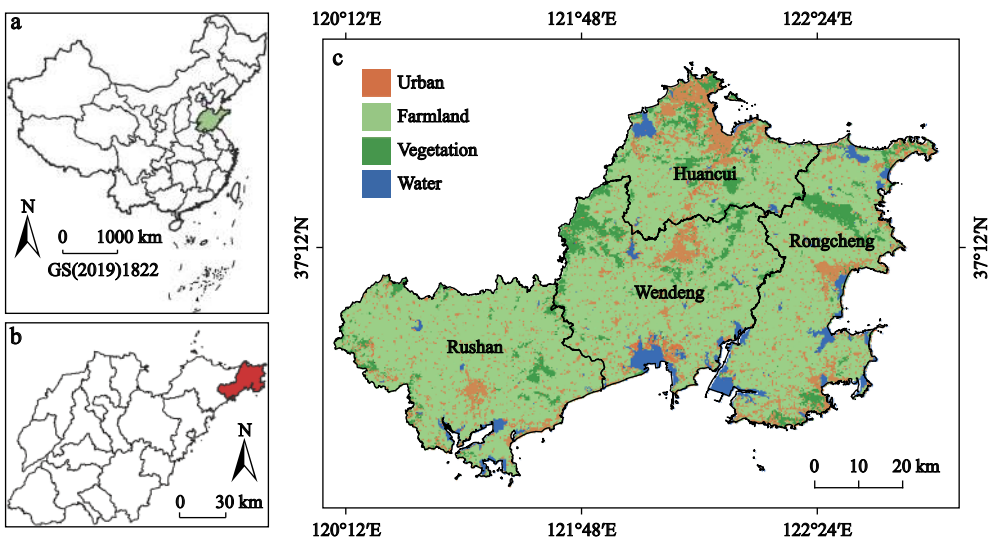

Fig. 1 Location of Shandong Province in China (a), location of Weihai County in Shandong (b), and administrative divisions of Weihai County (c)

CHIRPS, and Landsat data. All such data were obtained from the Google Earth Engine (GEE). The Moderate Resolution Imaging Spectroradiometer (MODIS) was developed by NASA (National Aeronautics and Space Administration) and operates from the Terra and Aqua satellite platforms. It provides 36 spectral bands ranging from the visible to the thermal infrared, with medium GSDs of 250–1000 m, observing the Earth's surface every one or two d. MODIS data products include three main types of land, atmosphere and ocean, and many standard products. For our study, we used MOD11A1 version 006 (a global 1-km surface temperature/emissivity L3 daily product) to derive the TCI, and MOD13Q1 version 006 (a global 250 m resolution vegetation index 16-d synthetic product) to deduce the VCI. The CHIRPS provides gridded precipitation datasets within 50°S and 50°N. The rasterized rain time series are created by a modeled combination of climatology data, satellite imagery, and meteorological site data for trend analysis and seasonal drought monitoring. The data resolution is 0.05° and the time span extends from January 1, 1981 to the present. Thus, we used long-term multi-temporal datasets of CHIRPS to calculate the RCI.

When developing an advanced comprehensive DCI from the above-mentioned three indices, the major challenge is to find the optimum coefficients. Although many researchers mentioned humidity as one of the most important parameters, this has been realized seldomly for model generation. So, we focused on the soil-relative humidity data obtained from the '10-day data set of crop growth and development and farmland soil moisture in China' of the China Meteorological Data Network (http://data.cma.cn) to calibrate our humidity based comprehensive model HcDCI.

To correlate and validate the CHIRPS precipitation data by the areal distribution and multi-temporal trends of surface water, such as rivers and reservoirs in the investigated region, October recordings of the years 2001 to 2019 which were evaluated by Landsat 5 TM, Landsat 7 ETM+, and Landsat 8 OLI with a GSD of 30 m and correlated with the accumulated precipitation measured from January to October. The model output was further validated by detailed agricultural crop yield data derived from the Weihai Statistical Yearbook (Bureau of Statistics of Weihai, 2002–2020).

To realize the automatic batch processing of the Landsat datasets, we used the ENVI 5.5 modeler function, and the administrative boundary vector was analyzed and mapped by the QGIS software. The processing of MODIS and CHIRPS data was mainly implemented by use of the Google Earth Engine (GEE), a cloud-based geospatial processing platform that can be used for the analysis of the global environment. The Earth Engine API supports Python and JavaScript, and thus, it was utilized to perform the necessary geospatial analysis.

2.3 Information extraction for model generation

2.3.1 Vegetation Condition Index (VCI)

Vegetation growth is closely related to the environmental development. The density and vitality of vegetation canopies are expressed by the difference in reflectance of spectral bands placed in the red (*RED*) and near-infrared (*NIR*) wavelengths that are provided by numerous satellite sensors and manifested as the 'red edge' phenomenon. NDVI reflects the presence, density, and vitality of vegetation canopies and indirectly reflects the environmental status. The lower the value of the NDVI (scaled between 0 and 1), the less (vital) vegetation is present (Rouse et al., 1974).

$$NDVI = \frac{NIR - RED}{NIR + RED} \tag{1}$$

The Vegetation Condition Index (VCI) is used to account for the vegetation growth and health during a period of time based on a long-term sequence (Kogan, 1995b). The formula to calculate the monthly scale monitoring is as follows:

$$VCI_i = \frac{NDVI_i - NDVI_{\min}}{NDVI_{\max} - NDVI_{\min}} \tag{2}$$

where the $NDVI_i$ is the value of the *NDVI* for the *i*-th month of a certain year, and $NDVI_{\min}$ and $NDVI_{\max}$ represent the minimum and maximum values, respectively, of the NDVI for the *i*-th month of many years. Therefore, the lower the VCI, the worse the vegetation density and vitality and the more severe the drought.

2.3.2 Temperature Condition Index (TCI)

Land Surface Temperature (LST), recorded by the MODIS sensor, corresponds to the temperature of the land surface, vegetation canopies, or that of water bodies. It is derived by emitted thermal infrared radiation. With rising temperatures, the transpiration of the soil and the evapotranspiration of vegetated areas is intensified and the loss of water will increase. In this context,

the 'Temperature Condition Index' (TCI) is used to evaluate the daytime temperature changes of land surfaces during a long period (Kogan, 1995a). The formula for monthly scale monitoring is as follows:

$$TCI_i = \frac{LST_{\max} - LST_i}{LST_{\max} - LST_{\min}} \tag{3}$$

where the LST_i is the value of the LST for the i-th month of a certain year, and $LST_{\min}$ and $LST_{\max}$ represent the minimum and maximum daytime values, respectively, for the i-th month of the selected years. Therefore, the lower the TCI, the higher the land surface temperature and the more severe the influence on the drought issue.

2.3.3 Rainfall Condition Index (RCI)

Precipitation data are the most important component of drought monitoring. Most scientists use normalized TRMM data or the data of the follow-on GPM mission. The spatial resolution of TRMM data is 0.25°, that of GPM is 0.1°, and CHIRPS data is provided at 0.05° since 1981. For our purposes, we decided to rely on the continuously produced and provided CHIRPS data to benefit from an improved spatial resolution. This study normalized the CHIRPS data and used it to calculate the *RCI* by the following formula:

$$RCI_i = \frac{CHIRPS_i - CHIRPS_{\min}}{CHIRPS_{\max} - CHIRPS_{\min}} \tag{4}$$

where the $CHIRPS_i$ is the value of $CHIRPS$ in the i-th month of a certain year, and $CHIRPS_{\min}$ and $CHIRPS_{\max}$ represent the minimum and maximum values, respectively, of CHIRPS for the i-th month of the selected years. Therefore, the smaller the RCI, the less the monthly precipitation and the higher the risk for a drought.

2.4 Generation of a comprehensive drought monitoring model

To create a comprehensive drought model, we linearly combined the three indices mentioned above—the VCI, the TCI, and the RCI to construct a basic Drought Condition Index (DCI) (Fig. 2).

$$\begin{aligned} &DCI = a \times VCI + b \times TCI + c \times RCI \\ &a + b + c = 1 \text{ and } a, b, c \in (0, 1) \end{aligned} \tag{5}$$

The essential task here is the determination of relevant model coefficients (a, b, and c). Various methods have already been used to determine these factors. However, most of those methods afford loads of measured field data and therefore are very complex and not easy to transfer to other regions. In our approach, we devised a less complex, but robust, reliable, and transferable solution including the possibility to model historical data. We found the China Meteorological Administration measures and used the 10–20 cm top soil relative humidity values as one of the classification standards for droughts (General Administration of Quality Super-

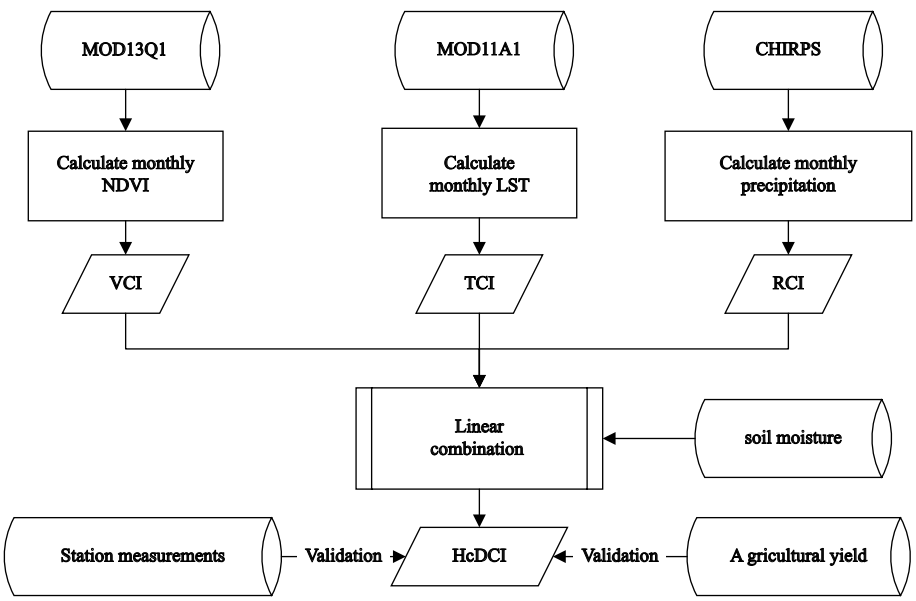

Fig. 2 Flowchart of the 'Humidity calibrated Drought Condition Index' (HcDCI) establishment based on a linear combination method. VCI, TCI, RCI is Vegetation Condition Index, Temperature Condition Index, Rainfall Condition Index. CHIRPS is Climate Hazards Group InfraRed Precipitation with Station data

vision et al., 2017). The uptake of water and nutrients is dependent on the penetration power of the roots. This is usually measured in terms of root length per cubic centimeter of soil. For winter wheat, the 10–20 cm upper soil layer has the highest root density and serves for efficient use of mineral nutrients and water and consequently reflects the water stress of the plants and the drought condition. Thus, we used the soil-relative humidity values of the China Meteorological Data Network (http://data.cma.cn) to determine the weight coefficients for our model.

The soil humidity data were provided from an agricultural station in Wendeng (No. 54777). The time range of available data reaches from June 1992 to June 2013, and each month was divided into the first, middle, and last 10 d. The relative humidity of the soil is divided into depths of 10, 20, 50, 70, and 100 cm. To calibrate our model, the humidity of the soil in 10 and 20 cm for each month (3 values) was averaged to get the relative humidity for the Wendeng Station from January 2001 to June 2013. After removing all invalid data, the total data amount was summed up to 135 mon. To calculate the model coefficients, a farmland closest to the Wendeng Station was selected. Then the spatially corresponding satellite data of this farmland area are used to calculate the index values of vegetation condition VCI (a), temperature condition TCI (b), and precipitation condition RCI (c) were computed using the GEE platform. The spatial resolutions of the respective datasets MOD11A1 (1 km), MOD13Q1 (250 m), and CHIRPS (0.05°) are different. GEE determines the scale of the analysis by the output. The system automatically uses the nearest neighbor method to resample the images to the output resolution before calculation (https://developers.google.com/earth-engine/guides/scale). To drive the factors for the proposed 'Humidity calibrated Drought Condition Index' model (HcDCI), 4851 combinations of a, b, and c in steps of 0.01 were calculated for 135 mon, respectively, to linearly fit the relative humidity of soil.

2.5 Methods of validation

2.5.1 Correlation of precipitation, station measurements and surface water area

For validation purposes, a correlation between precipitation data from CHIRPS and the respective water area was desired, although there are neither big rivers nor big lakes in Weihai County. The main surface water-gathering areas are reservoirs and medium as well as small rivers. With reference to the 'Hydrological Information Network' (http://www.whsw.info) and the administrative map of Weihai County, 43 reservoirs and 8 rivers (parts of the river section) were selected for analysis. The runoff is affected by the precipitation in the respective season, and the flow is often interrupted in the dry period. The largest rivers flow through all four districts. These include the drainage area of the Muzhu River and the Rushan River with more than 1000 km^2. The overall lengths of the Muzhu River, the Rushan River, and the Huanglei River is more than 60 km. The most promising time to gather the fluctuations in surface water levels turned out to be shortly after the main rainy season. Thus, Landsat data recorded each October from 2000 to 2019 were selected, apart from the years 2011, 2016, and 2018 due to a lack of cloud free data. Data were atmospherically and radiometrically pre-processed, and the outside border of the research area was masked. Then an unsupervised classification approach was used to calculate the area covered by water bodies.

2.5.2 Correlation of HcDCI values with yield

The most significant diagnostic approach to prove the quality of the results derived from our model is to correlate the drought events over a period of time with different crop subsequently harvested. To correlate the HcDCI results with agricultural yield data, we consulted the Weihai Statistical Yearbook (Bureau of Statistics of Weihai, 2002–2020). Quantitative yield data for the years 2001–2018 are available as area-related, as total yield, and as per square meter of crop (kg/m^2). The unit of production is given in tons. In different years, the unit of area is provided in acres and hectares that we converted to kg/m^2. In most years, the planting area of grain crops reached between 60%–70% compared to vegetables and other crops. The yield per square meter of grain is separated in those harvested in summer (mainly winter wheat sown in October) and others harvested in autumn (mainly corn and peanuts sown in June). We used both the data of summer and fall harvests for correlation with the HcDCI.

3 Results

3.1 NDVI/VCI development and trend

The inter-annual development of the NDVI is displayed

in Fig. 3a. From 2001 to 2019, the average value of the NDVI of Weihai County was 0.3822. The minimum value of 0.3518 shows up in 2001, while the maximum value of 0.4092 was measured in 2018. The general trend in the investigated time period was increasing. The linear fitting formula is $y = 0.001x + 0.365$, and the r value (correlation coefficient) results in 0.6626.

The spatial distribution of the averaged NDVI values is shown in Fig. 3b. The derived VCI values in August 2019 expectedly depict a similar scheme, that is displayed in Fig. 3c.

3.2 Temperature development and trend

The inter-annual changes of the temperature are shown in Fig. 4a. The annual average temperature of Weihai County continued to rise slightly from 2012 to 2019. This can be attributed to global warming with a minor contribution of urban sprawl. The annual average temperature during the past eight years was 13.57°C, about 1°C higher than during the averaged time period from 2001 to 2011. The average temperature during 2001–2019 was 12.96°C. The average temperature at daytime resulted to 19.44°C, while the average temperature at night was 6.47°C. The average temperature difference between day and night was 12.97°C.

The spatial distribution of averaged day and night LSTs is shown in Figs. 4b and 4c. The temperatures of forest, coastal, and inland waters are lower during daytime, and higher during nighttime. The temperature differences between day and night in the Rushan area are larger than those in the other three districts. Fig. 4d shows the TCI in August 2019 calculated from daytime temperatures (Fig. 4b).

3.3 Precipitation changes and trend

The inter-annual changes of precipitation are given in Fig. 5a, indicating significant fluctuations. The average value of precipitation in 19 yr was 719.80 mm/yr. The minimum value of 507.95 mm showed up in 2002, while the maximum value of 956.02 mm was measured in 2007. The precipitation rate in the past six years (2014–2019) was lower than that the years before. It shows an average value of 615.53 mm, indicating a decrease of 192.77 mm from 808.29 mm in the previous six years (2008–2013). Precipitation is mostly concentrated in July and August, reaching 48.58% of the total year. There are seven months with less than 40 mm preciptationl, including less than 20 mm preciptationin January, February, and March.

The spatial variations of average precipitation are shown in Fig. 5b. The precipitation in Weihai shows a significant decreasing trend from southwest to northeast with certain spatial differences. The average precipitation in the north of Rongcheng is about 650 mm, while

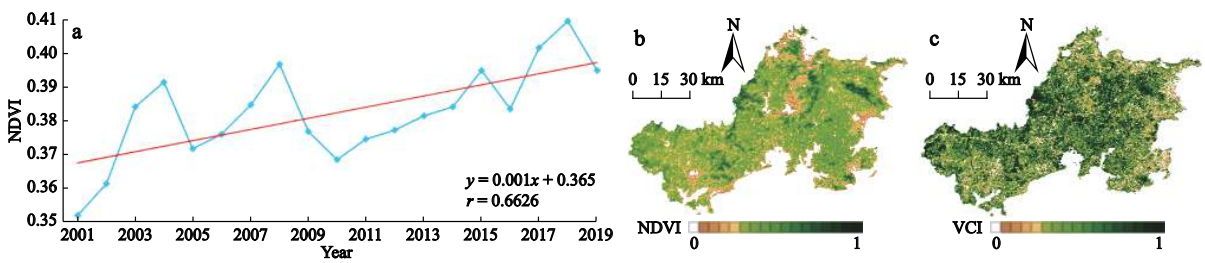

Fig. 3 Annual change of the Normalized Difference Vegetation Index (NDVI) from 2001 to 2019 (a), averaged NDVI values (b), Vegetation Condition Index (VCI) values derived from NDVI in August 2019 (c) in Weihai County, Shandong Province, China

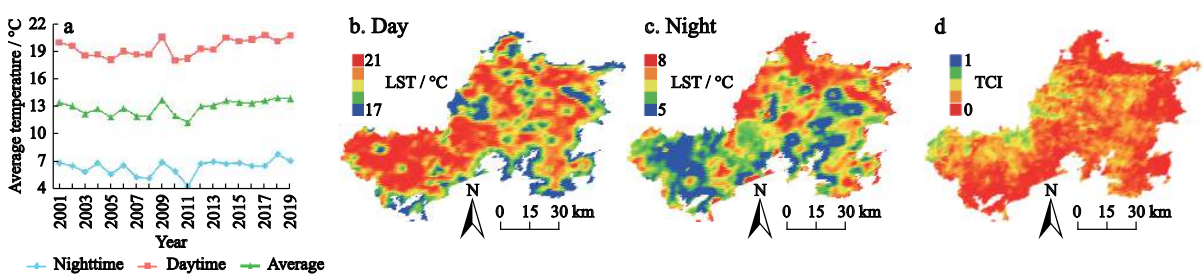

Fig. 4 Annual changes of Land Surface Temperatures (LSTs) from 2001 to 2019 (a), spatial distribution of averaged day and night LSTs (b, c), Temperature Condition Index (TCI) in August 2019 derived from daytime temperatures (d) in Weihai County, Shandong Province, China

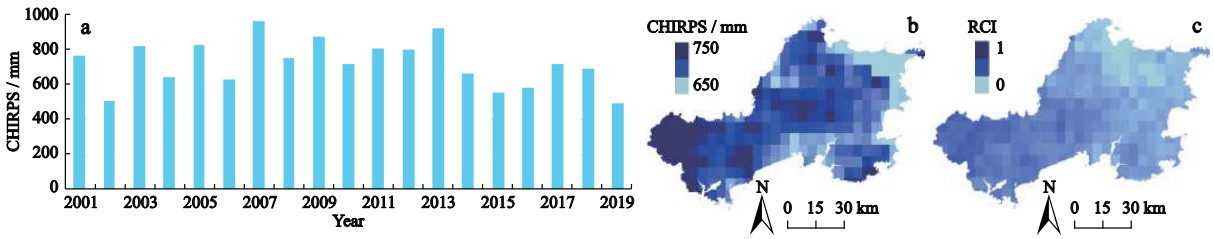

Fig. 5 Annual fluctuations in precipitation from 2001 to 2019 (a), spatial variations of average precipitation (b), Rainfall Condition Index (RCI) in August 2019 calculated from precipitation data (c) in Weihai County, Shandong Province, China

the average precipitation in the west of Rushan is about 800 mm. Fig. 5c displays the RCI in August 2019 calculated from the respective precipitation data.

3.4 HcDCI, relative humidity and drought levels

First the variables VCI, TCI, and RCI are combined to a basic DCI that shows a significant positive correlation with the 10–20 cm top soil relative humidity. Hence, we determined the respective coefficients for the model based on the given humidity data. The correlation coefficient turns out to be highest at 0.6710, when VCI, TCI, and RCI are 0.53, 0.33, and 0.14 respectively ($P < 0.01$). The fitting effect with this combination of coefficients is given in Fig. 6.

The corresponding relationship between the relative humidity values of the 10–20 cm top soil and the drought levels is proposed in grades used for meteorological droughts (General Administration of Quality Supervision et al., 2017). The corresponding HcDCI levels are calculated by the linear fitting formula $y = 0.008x - 0.056$, and the results are shown in Table 1.

3.5 Spatio-temporal distribution and strength of droughts

The general agricultural drought development in Weihai County, as modeled by the HcDCI, reveals no to light droughts during the time period 2003 till 2013, and in 2018. It also uncovers light to severe droughts in 2001 and 2002, from 2014 to 2017, and in 2019 (Fig. 7). The modeled data coincides with available historical records. Furthermore, it is obvious that severe droughts occurred in a well-balanced way throughout all the four quarters of the respective years and increased significantly since 2014, with the sole exception of 2018.

The spatial distribution of droughts (averaged per year) in Weihai County from 2001 to 2019 is shown in Fig. 8. The occurrence of droughts is random with no focus at a specific district or area. In 2001, light and severe droughts transpired throughout the investigated area, with most severe droughts in the Rongcheng and Rushan areas. In 2002, the drought situation eased, but it still remained severe in the Rushan District. A small drought occurred in 2004 with a more severe character in Rushan. In 2006, 2007, and 2009, small-scale, light droughts arose with a relatively scattered distribution. In 2014, 2015, and 2016, medium-sized droughts occurred throughout the four districts of Weihai County. In 2014, droughts concentrated in Huancui and Rongcheng, while Rushan and West-Wendeng faced the same situation in 2015. In 2017, Huancui, Rongcheng, and Wendeng experienced light to moderate droughts, but there was no large-scale drought in Rushan. In 2019, light droughts occurred throughout the four districts,

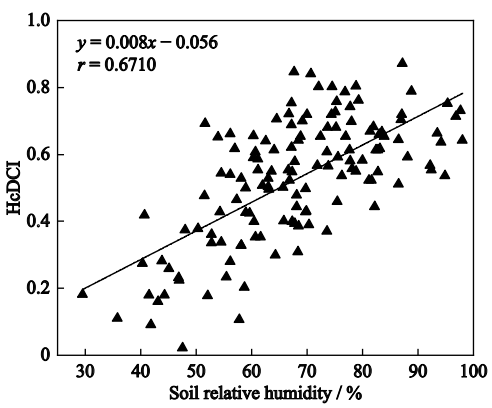

Fig. 6 Fitting diagram of HcDCI and the relative humidity of the soil at the Wendeng station, Shandong Province, China

Table 1 Criteria for drought classification

Level	Relative humidity	HcDCI	Drought level
1	>60	>0.424	No
2	50–60	0.344–0.424	Light
3	40–50	0.264–0.344	Moderate
4	30–40	0.184–0.264	Severe
5	<30	<0.184	Extreme

Note: HcDCI: 'Humidity calibrated Drought Condition Index'

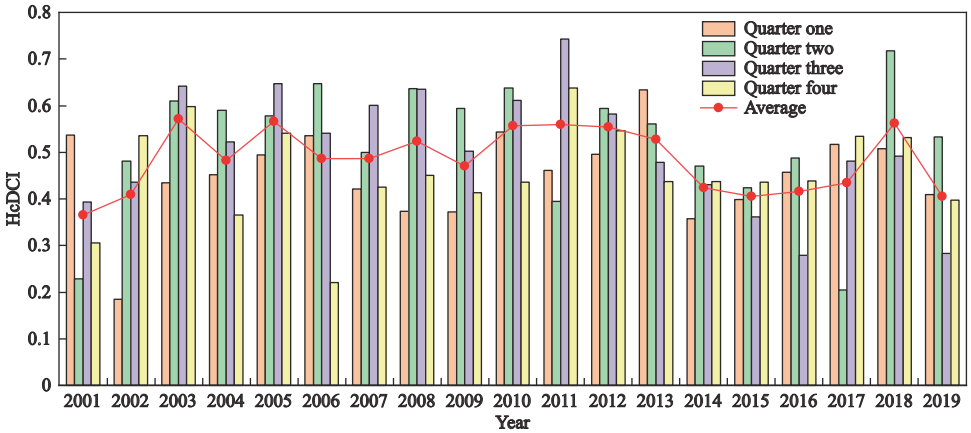

Fig. 7 Inter-annual changes and trends of the HcDCI of Weihai County, Shandong Province from 2001 to 2019 separated into four seasons (quarters) every year. Quarter one: January to March; Quarter two: April to June; Quarter three: July to September; Quarter four: October to December

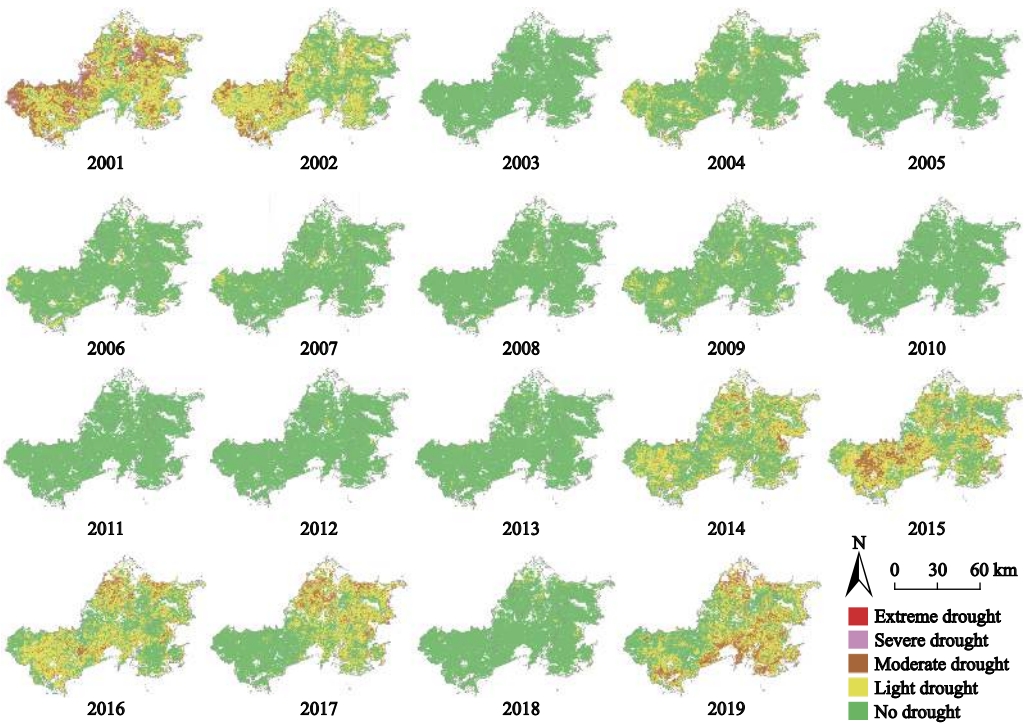

Fig. 8 Spatial changes of agricultural droughts in Weihai County, Shandong Province, China from 2001 to 2019

while moderate droughts emerged in the northern part of Huancui, South-Rongcheng, South-Wendeng and South-Rushan. Table 2 displays the relative proportions of drought levels for the entire investigated area and time period.

The monthly changes in drought levels are realized by averaging the HcDCIs of all months from 2001 to 2019 (Fig. 9). Data show that from 2001 to 2019 repeated droughts occurred, with emphasis on January, March, November, and December for the entire area. The months of relatively obvious, but more scattered drought events in various districts are: April and September in Huancui, September in Rongcheng, July and September in Wendeng, and February and October in Rushan.

The range of the drought level reaches from about 0.38 to 0.51. The droughts in January, March, and December are more severe, and those happened from September to December continue to intensify with a major strength in spring and winter.

3.6 Validation of results

The accuracy of the developed model is primarily con-

Table 2 Proportion of drought areas at various levels in drought years in Weihai County, Shandong Province, China / %

Year	Drought Level					Disaster proportion
	No drought	Light drought	Moderate drought	Severe drought	Extreme drought	
2001	13.4413	52.8318	30.8264	2.8899	0.0106	86.5587
2002	36.7414	54.1438	9.0687	0.0376	0.0084	63.2586
2004	85.5812	14.0230	0.3726	0.0102	0.0131	14.4188
2006	94.2493	5.6475	0.0889	0.0095	0.0048	5.7507
2007	95.2890	4.6270	0.0775	0.0028	0.0037	4.7110
2009	88.6485	11.2261	0.1126	0.0124	0.0004	11.3515
2014	52.6272	42.4350	4.7637	0.1642	0.0099	47.3728
2015	38.2693	47.7612	13.5148	0.4424	0.0123	61.7307
2016	42.8918	49.1723	7.6901	0.2380	0.0078	57.1082
2017	56.0192	35.6063	7.7936	0.5614	0.0195	43.9808
2019	38.9641	43.8469	15.8805	1.2982	0.0103	61.0359

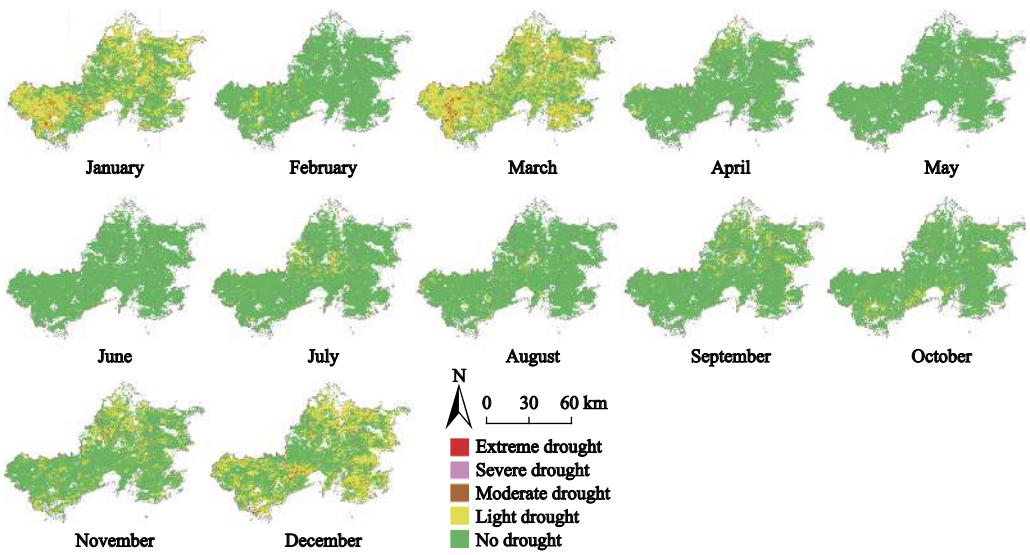

Fig. 9 Average monthly agricultural droughts in Weihai County, Shandong Province, China during 2001–2019

trolled by the precipitation data and the availability and quality of the measured and archived humidity data. The remaining inputs, such as VCI and TCI, are from their nature data sources with very high confidence. Therefore, we focused the validation procedures on the RCI model input concerning the used CHIRPS estimates in relation to precipitation measurements of ground station data and to the extension of surface water areas, while the model output was compared to the statistical records of the respective agricultural crop yields.

3.6.1 CHIRPS values related to station data and the surface water area

To validate the accuracy of CHIRPS data, we first compared them to the local measurements of ground stations in Weihai County. Then, we further matched them with the expansion of the surface water area derived from high-resolution optical satellite data. The area covered by surface water varies greatly over the years with a maximum difference of 38.68 km^2. The minimum value of the surface water area appeared in 2000, while the maximum value is exposed in 2007. The surface water area in 2000 accounted for only 30.37% in 2007. The variations in the individual districts are well balanced, although the Wendeng District faced the strongest reduction of the surface water area by about 25% since 2015.

According to the analysis of the ground station data, provided by the Statistical Yearbook of Weihai (Bureau

of Statistics of Weihai, 2002–2020), the average precipitation in Weihai County reached 1124.2 mm in 2007. This was the highest value ever recorded. From January to October 2019, the cumulative precipitation in Weihai County reached 371.3 mm, that was 42.4% less than the preciptation in the same season the year before and 47.0% less than during the same season in many years.

To be able to compare CHIRPS data and ground-measured precipitation data with the recorded surface water area, the cumulative precipitation from January till October was calculated for each year from 2001 to 2019 for all data sources. Fig. 10 displays the cumulative precipitation provided by CHIRPS and the ground stations in combination with a line chart, marking the surface water area. The trends of precipitation and surface water area are significantly similar, although the illustration exhibits some minor discrepancies in detail. CHIRPS data of the years 2009 and 2013 do not well match the overall trend function of stationary measurements and the surface water area. Furthermore, the ground stations display a slightly higher preciptation amount in contrast to the CHIRPS data during the first half of the entire time period, with an opposite trend during the second half. In this context, it can be suspected that CHIRPS did not manage to download the station data in China routinely.

The linear fitting result based on two sources of precipitation data and the surface water area are shown in Fig. 11. The correlation coefficient between the station measurements and the surface water area is strongest at 0.7664 ($P < 0.01$). The correlation coefficients between the CHIRPS data and the variables 'station-precipitation' and 'surface water area' are of high to moderate degrees and can be considered as a reliable magnitude of association. Additionally, we correlated the surface water area acquired every year in October with the HcDCI calculated for the third quarter of each year. The correlation coefficient resulted to 0.6504 ($P < 0.01$) from which can be deduced that the statistical results between the HcDCI and the surface water area have certain credibility.

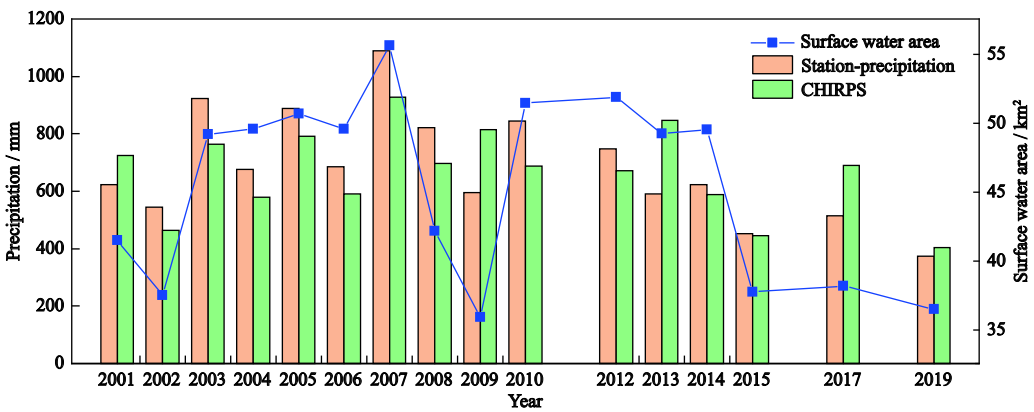

Fig. 10 Cumulative precipitation measured by CHIRPS and local ground stations, coupled with a line chart marking the surface water area in Weihai County from 2001 to 2019. Data of 2011, 2016 and 2018 are missing due to the lack of cloud free data of Landsat in October

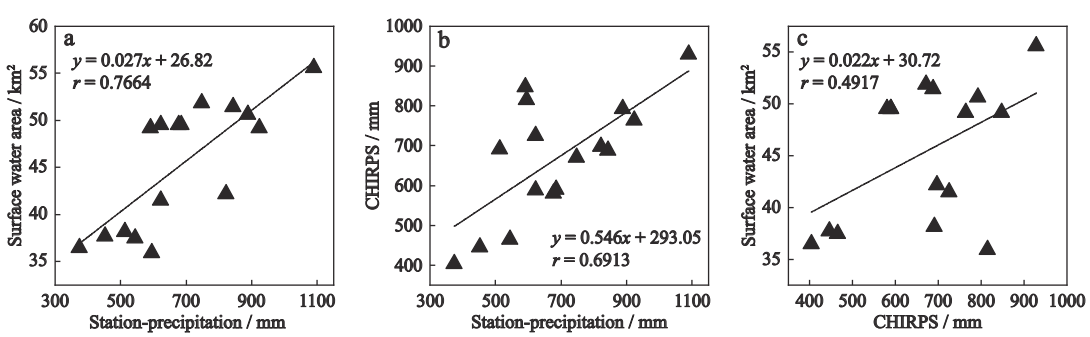

Fig. 11 Correlation coefficients between station data and surface water area (a), station data and CHIRPS data (b), and surface water area and CHIRPS data (c)

3.6.2 HcDCI values related to the achieved agricultural yield

To further validate the accuracy of the developed HcDCI, the calculated varying drought indices were correlated with the amount of grain yield data achieved. The Weihai Statistical Yearbook (Bureau of Statistics of Weihai, 2002–2020) provides the total yield area, total yield, and the yield per square meter for different crops from 2001 till 2019. The crop yield data is partitioned into grown crops such as grain crops, peanuts, vegetables, medicinal materials, and melons, among others, where grain crops (winter wheat and corn) cover about 65% of the agricultural fields. To examine the correlation between the HcDCI and the crop yield of winter wheat and corn, we used two different inputs (Figs. 12a–12d). One was realized by correlating the respective yield with the drought indices of the two previous quarters of the year before harvesting. This coincides with the jointing, heading, and filling stages of the grain crops. This is also the critical period of water demand. In a second attempt, the yield of both crop types was correlated with the HcDCI of the entire growth period. Both approaches for the distinct crop types exhibit a significant coherency, where the results based on the two preceding months of the HcDCI perform best and winter wheat performs better than corn. All calculations passed the significance test ($P < 0.01$) and approved the HcDCI to be a useful tool for drought monitoring in rainfed agricultural areas.

4 Discussion

As far as the primary inputs of our model are concerned, all variables are characterized by a high confidence. This is especially true for the TCI and VCI, as those are synoptically recorded by satellite sensors since many years with an accuracy not measurable in such areal detail by ground stations. However, the VCI is not classified with reference to distinct crop types but to the density and the state of vitality of vegetation. Therefore, uncertainties may arise if there are no monocultures but the presence of additional crops, such as vegetables, peanuts and more. Their specific spectral reflectance additionally modifies the NDVI and, thus, the VCI component, but they are not considered concerning the crop yield. This issue is especially true for the summer cultivation of corn, that depicts a lower correlation to the HcDCI values than the winter wheat. Besides, the varying drought tolerances of each crop in different growth stages, along with possible scattered infections and a selective fertilization, are also not considered so far. Moreover, though Weihai County is dominated by rainfed agriculture, some regions rely on irrigation schemes that may change in space and time and can further negatively affect the results. In this context, further attempts have to be made in the future to include crop type, fertilization and irrigation schemes to improve the validation procedure and the accuracy of results.

For the validation based on crop yield, we faced tolerable constraints concerning the respective method of how yield data had been collected. In our case, the survey method changed in 2014 from where the quantitative yield data is consistent in itself, but it is not comparable to the data of previous years. Before 2014, the results of the areas under cultivation were reported by local yields on the village, town, and county levels. After 2014, data were obtained by statisticians through UAV (Unmanned Aerial Vehicle) or satellite data. Since the amount of crop yield data, especially of the years 2014 and 2015, could not be explained in the context to former harvests, we used the crop yield data from 2001 to 2013 for the validation.

The third input variable, the RCI is the most critical of all. Ground station data are highly accurate but lack area-covering measurements. TRMM and CHIRPS data from satellite recordings are quite reliable, and offer a reasonable accuracy, whereby CHIRPS data benefit of a merge with ground measurements (Funk et al., 2015). Although, our validation approach with the varying areal coverage of surface waters such as rivers and lakes resulted in an acceptable correlation with CHIRPS and local ground measurements, there cannot be a linear relationship due to naturally varying slope angles of riverbanks and lakeshores. Including bathymetric data for the region of interest might improve the validation procedure and consecutively offer more confidence in the RCI input variable. A further improvement might be feasible by using microwave data from recently launched satellite sensors which can deeper penetrate into the soils than optical sensors and thus, provide frequent synoptic measurements of soil moisture (Sawada et al., 2019; Zhang et al., 2019). The core challenge of our drought model is the determination of the weight coefficients for the basic inputs VCI, TCI, and RCI and the choice of the calibration method. As many researchers consider soil humidity as one of the most important

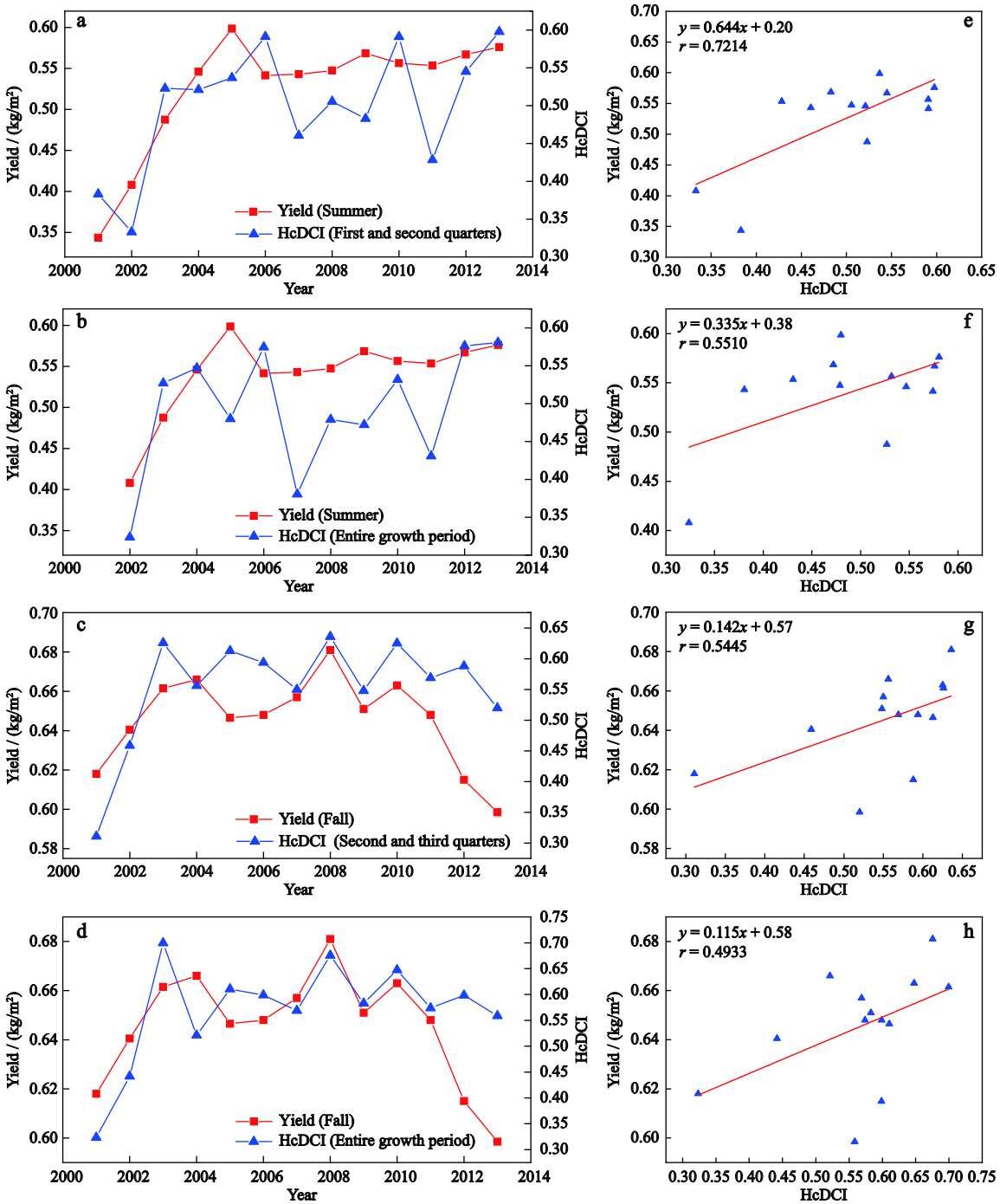

Fig. 12 Correlation and relationship between the total yield of summer (winter wheat) and fall (corn) with the HcDCI calculated for different quarters of the year from 2001 to 2013 in Weihai County. Summer harvest and HcDCI of the 1st and 2nd quarter of the year (a, e) and the entire growth period (b, f). Fall harvest and HcDCI of the 2nd and 3rd quarter of the year (c, g) and the entire growth period (d, h)

variables for drought monitoring (Eswar et al., 2018; Sazib et al., 2018; Mladenova et al., 2020), we decided to establish the model coefficients based on locally measured humidity data. Apart from minor constraints in model generation and validation, the integration of soil humidity values for model calibration turned out to be very reasonable and successful. Those data are most confident, are available in most countries and control the reliability and accuracy of the model and the corresponding results. Possible improvements in this context

may be achievable by choosing the optimum depth where humidity data are measured to precisely adapt these levels to the root level of the respective crops (Menge et al., 2016). Although, ground measurements of soil humidity data are available in many countries, respective stations are often widely scattered and data are measured rather infrequently. Therefore, we also calculated the respective coefficients between HcDCI (using Wendeng station data to determine the coefficients) and the humidity of stations in Fushan and Laiyang which are located outside Weihai County in the neighboring Yantai District. The results turned out to be reasonable with coefficients of 0.4438 and 0.3619 along with a $P < 0.01$, but the accuracy decreased seriously. Hence, the transferability of the model is given as compared to principal component (PCA) and neural network (NN) approaches (Kaur and Sood, 2020; Kim et al., 2021), but measurements of the closest local database are absolutely favored for calibration purposes.

5 Conclusions

In order to confirm and analyze the worldwide increased occurrence of droughts in the eastern China, we have developed a comprehensive modeling approach based on remotely recorded satellite data from 2001 to 2019. This was realized with the help of distinct indices that were calculated from MODIS satellite data and the CHIRPS system. The three most influential factors determined are the vitality and distribution of vegetation (VCI), the localities and level of land surface temperatures (TCI) and the distribution and level of precipitation (RCI). It was found that the annual average temperature of Weihai County continuously raised from 2012 to 2019 what can be attributed to global warming with a minor contribution of urban sprawl. The general trend of the VCI based on the NDVI was also increasing in the investigated time period while the precipitation index (RCI) showed no trend but varied significantly from year to year. Higher precipitation is mostly concentrated in July and August, while in January, February, and March the preciptation is less than 20 mm. These three variables VCI, TCI, and RCI are combined to a basic DCI that shows a significant positive correlation with the 10–20 cm top soil relative humidity measured by an agrometeorological ground station and, thus, was consequently used to determine the respective coefficients for our model. The corresponding HcDCI (Humidity calibrated DCI) levels are given in grades used for meteorological droughts. The new model was then applied to the Weihai County region characterized by huge areas of rainfed agriculture. The occurrence of droughts turned out to be random with no focus at a specific district or area. Light and severe droughts transpired throughout the investigated area most significantly in 2001 and 2002, 2014–2017, and 2019. Repeated droughts occurred with emphasis on January, March, and December for the entire area.

The thoroughly accomplished validation procedures revealed the newly developed model as sufficiently accurate when using three basic indices as input variables, especially CHIRPS data for precipitation and ground based humidity data for calibration. Therefore, in the future, the developed HcDCI will be used for operational monitoring of agricultural droughts in Weihai County, Shandong Province, China. We conclude that the developed 'Humidity calibrated Drought Condition Index' and its findings provide clear quantitative evidence of its robustness and applicability for monitoring agricultural drought events, offers forecasting options, and helps to contribute to the understanding of a respective ecological status and its evolution.

The validation of the derived results was a most challenging issue. Concerning uncertainties with the CHIRPS data we correlated them with the ground-measured cumulative precipitation from January till October and the surface water area recorded by Landsat satellites. The correlation coefficients are of high to moderate degrees and can be considered as a reliable magnitude of association. The same is true for the correlation of the surface water area acquired every year in October with the HcDCI calculated for the third quarter of each year. The accuracy of the developed HcDCI was further positively validated by correlating the varying drought indices with the amount of winter wheat and corn yield.

References

Bureau of Statistics of Weihai, 2002–2020. *Weihai Statistical Yearbook* (2001–2019). (in Chinese)

Chen Weiying, Xiao Qianguang, Sheng Yongwei, 1994. Application of the anomaly vegetation index to monitoring heavy drought in 1992. *Journal of Remote Sensing*, 9(2): 106–112. (in Chinese)

Choi M, Jacobs J M, Anderson M C et al., 2013. Evaluation of drought indices via remotely sensed data with hydrological variables. *Journal of Hydrology*, 476: 265–273. doi: 10.1016/

j.jhydrol.2012.10.042

Du L T, Tian Q J, Yu T et al., 2013. A comprehensive drought monitoring method integrating MODIS and TRMM data. *International Journal of Applied Earth Observation and Geoinformation*, 23: 245–253. doi: 10.1016/j.jag.2012.09.010

Eswar R, Das N N, Poulsen C et al., 2018. SMAP soil moisture change as an indicator of drought conditions. *Remote Sensing*, 10(5): 788. doi: 10.3390/rs10050788

Funk C, Peterson P, Landsfeld M et al., 2015. The climate hazards infrared precipitation with stations—a new environmental record for monitoring extremes. *Scientific Data*, 2(1): 1–21. doi: 10.1038/sdata.2015.66

General Administration of Quality Supervision, Inspection and Quarantine of the People's Republic of China, Standardization Administration of the People 's Republic of China, 2017. Grades of meteorological drought: GB/T 20481-2017. Beijing: Standards Press of China. (in Chinese)

Huete A R, Liu H Q, Batchily K et al., 1997. A comparison of vegetation indices over a global set of TM images for EOS-MODIS. *Remote Sensing of Environment*, 59: 440–451. doi: 10.1016/s0034-4257(96)00112-5

Idso S B, Jackson R D, Pinter P J et al., 1981. Normalizing the stress-degree-day parameter for environmental variability. *Agricultural Meteorology*, 24: 45–55. doi: 10.1016/0002-1571(81)90032-7

Kaur A, Sood S K, 2020. Cloud-Fog based framework for drought prediction and forecasting using artificial neural network and genetic algorithm. *Journal of Experimental & Theoretical Artificial Intelligence*, 32(2): 273–289. doi: 10.1080/0952813X.2019.1647563

Kim J E, Yu J, Ryu J H et al., 2021. Assessment of regional drought vulnerability and risk using principal component analysis and a Gaussian mixture model. *Natural Hazards*, 2021: 1–18. doi: 10.1007/s11069-021-04854-y

Kogan F, 2002. World droughts in the new millennium from AVHRR-based vegetation health indices. *Eos Transactions, American Geophysical Union*, 83(48): 557–563. doi: 10.1029/2002EO000382

Kogan F N, 1995a. Application of vegetation index and brightness temperature for drought detection. *Advances in Space Research*, 15(11): 91–100. doi: 10.1016/0273-1177(95)00079-T

Kogan F N, 1995b. Droughts of the late 1980s in the United States as derived from NOAA polar-orbiting satellite data. *Bulletin of the American Meteorological Society*, 76(5): 655–668. doi: 10.1175/1520-0477(1995)076<0655:DOTLIT>2.0.CO;2

Li X, Zhou W, Chen Y D, 2015. Assessment of regional drought trend and risk over China: a drought climate division perspective. *Journal of Climate*, 28(18): 7025–7037. doi: 10.1175/JCLI-D-14-00403.1

Lu Y, Hu H, Li C et al., 2018. Increasing compound events of extreme hot and dry days during growing seasons of wheat and maize in China. *Scientific Reports*, 8(1): 1–8. doi: 10.1038/s41598-018-34215-y

McKee T B, Doesken N J, Kleist J, 1993. The relationship of drought frequency and duration to time scale. *In:Proceedings of the 8th Conference on Applied Climatology. Anaheim:American Meteor Society*, 179–183.

McVicar T R, Jupp D L, 2002. Using covariates to spatially interpolate moisture availability in the Murray-Darling Basin: a novel use of remotely sensed data. *Remote Sensing of Environment*, 79(2--3): 199–212. doi: 10.1016/S0034-4257(01)00273-5

Menge D M, Kameoka E, Kano-Nakata M et al., 2016. Drought-induced root plasticity of two upland NERICA varieties under conditions with contrasting soil depth characteristics. *Plant Production Science*, 19(3): 389–400. doi: 10.1080/1343943X.2016.1146908

Mladenova I E, Bolten J D, Crow W et al., 2020. Agricultural drought monitoring via the assimilation of SMAP soil moisture retrievals into a global soil water balance model. *Frontiers in Big Data*, 3: 10. doi: 10.3389/fdata.2020.00010

Palmer W C, 1965. *Meteorological Drought*. US Weather Bureau Research Paper-No. 45. Washington: Office of Climatology U. S. Weather Bureau

Price J C, 1985. On the analysis of thermal infrared imagery: the limited utility of apparent thermal inertia. *Remote Sensing of Environment*, 18: 59–73. doi: 10.1016/0034-4257(85)90038-0

Qi Shuhua, Wang Changyao, Niu Zheng et al., 2004. SVI and VCI based on NDVI time-series dataset used to monitor vegetation growth status and its response to climate variables. *Progress in Geography*, 23(3): 91–99. (in Chinese)

Rhee J, Im J, Carbone G J, 2010. Monitoring agricultural drought for arid and humid regions using multi-sensor remote sensing data. *Remote Sensing of Environment*, 114(12): 2875–2887. doi: 10.1016/j.rse.2010.07.005

Rouse J W Jr, Haas R H, Schell J A et al., 1974. Monitoring vegetation systems in the Great Plains with ERTS. *In:Goddard Space Flight Center 3d ERTS-1 Symposium. Washington: NASA*, 309–318.

Sandholt I, Rasmussen K, Andersen J, 2002. A simple interpretation of the surface temperature/vegetation index space for assessment of surface moisture status. *Remote Sensing of Environment*, 79(2-3): 213–224. doi: 10.1016/s0034-4257(01)00274-7

Sawada Y, Koike T, Ikoma E et al., 2019. Monitoring and predicting agricultural droughts for a water-limited subcontinental region by integrating a land surface model and microwave remote sensing. *IEEE Transactions on Geoscience and Remote Sensing*, 58(1): 14–33. doi: 10.1109/TGRS.2019.2927342

Sazib N, Mladenova I, Bolten J, 2018. Leveraging the Google Earth Engine for drought assessment using global soil moisture data. *Remote Sensing*, 10(8): 1265. doi: 10.3390/rs10081265

Van Rooy M P, 1965. A rainfall anomaly index independent of the time and space. *Notos*, 14: 43–48.

Wardlow B D, Anderson M C, Verdin J P, 2012. Drought monitoring: historical and current perspective. In: Wardlow B D et al. (eds). *Remote Sensing of Drought*. Boca Raton: CRC Press. doi: 10.1201/b11863-8

West H, Quinn N, Horswell M, 2019. Remote sensing for drought monitoring & impact assessment: progress, past challenges and future opportunities. *Remote Sensing of Environment*, 232: 111291. doi: 10.1016/j.rse.2019.111291

Zhang A Z, Jia G S, 2013. Monitoring meteorological drought in semiarid regions using multi-sensor microwave remote sensing data. *Remote Sensing of Environment*, 134: 12–23. doi: 10.1016/j.rse.2013.02.023

Zhang A, Jia G, Wang H, 2019. Improving meteorological drought monitoring capability over tropical and subtropical water-limited ecosystems: evaluation and ensemble of the Microwave Integrated Drought Index. *Environmental Research Letters*, 14(4): 044025. doi: 10.1088/1748-9326/ab005e